NUMERICAL INVESTIGATION ON THE AERODYNAMICS OF A TUNNEL VENTILATION FAN DURING PRESSURE PULSES

D. Borello[1] - A. Corsini[1] – G. Delibra[1] – F. Rispoli[1]– A. G. Sheard[2]

[1]Dip. di Ingegneria Meccanica e Aerospaziale, *Sapienza* University of Rome, Italy

[2]FlaktWoods Ltd, Colchester, UK

ABSTRACT

The paper reports on the simulation of a ventilation fan under pressure pulses generated by train passages in tunnel and metro systems. Such pulses alter the volume flow rate through the fan, and consequently the overall aerodynamics, causing structural stress, vibrations, and forcing the unit to operate off-design. A proper understanding of the unsteady aerodynamics during the pressure fluctuations is mandatory to obtain useful guidelines to fan designers. Here the pressure waves due to train passage are modelled as a region of rapidly changing volume flow rate. The fan operation are computed with a large eddy simulation (LES) one-equation sub-grid scale (SGS) model implemented in the open source code OpenFOAM. This investigation provides an insight of the effects on the turbulent structures developing along the fan blades, as well as the conspicuous detrimental effect on the aerodynamics of the fan.

NOMENCLATURE

$<c_{SGS}>$	[-]	Smagorinsky coefficient
k_{SGS}	[m^2/s^2]	sub-grid turbulent kinetic energy
y^+	[-]	normalised wall distance
C_p	[-]	pressure coefficient. $C_p=(p-p_0)/U_{tip}$
D_{tip}	[m]	tip diameter
P_{kSGS}	[m^2/s^3]	production of k_{SGS}
Q	[$1/s^2$]	vortex eduction parameter. $Q=0.5(\Omega_{ij}\,\Omega_{ij}- S_{ij}S_{ij})$
R	[m]	radius
U_{bulk}	[m/s]	bulk velocity
U_{tip}	[m/s]	tip velocity
V	[m^3]	cell volume
W	[m/s]	relative velocity
ε_{kSGS}	[m^2/s^3]	sub-grid scale dissipation of k
ν	[m^2/s]	molecular kinetic viscosity
ν_{SGS}	[m^2/s]	sub-grid scale viscosity
ω	[1/s]	angular velocity
$\Delta=V^{1/3}$	[m]	LES length-scale

INTRODUCTION

The evolution of industrial design of fan units in metropolitan mass-transfer systems is driven by twofold elements. On the one hand, the compliance with the harmonised standard EN 12101-3, incorporated into the ISO 21927-3 [1], on the other, the capability to adapt the aerodynamic performance to different operating scenarios, i.e. the extraction of hot air and gas at 400°C in emergency operations or the coupling with pressure fluctuations within the tunnel systems in normal operation. Both factors pushed the industry towards more advanced design methodologies based on CFD analysis and virtual prototyping techniques, derived from aerospace practice [2]. The operat-

ing requirements lead inevitably to a series of compromises in the design of fans that limits their aerodynamic performance. Specifically, the design and selection of tunnel and metro fans need to take into account their peculiar installation, that is characterised by a series of pressure pulses generated by the passage of trains. Such pulses alter the volume flow rate through the fan, and consequently the fan unit is forced to work in an operating envelope larger than the design one. The operating maps of fans are limited by the occurrence of aerodynamic instabilities which place considerable mechanical stress on the rotors and eventually lead to mechanical failure by rapid fatigue. As demonstrated by Rippl (1995)[3], alternating stress in blade vanes exceeded stable operation by a factor of five under unstable conditions due to rotating stall.

Fan designers classically produce a mechanical design that can withstand the alternating loads imposed on the fan blades associated with rotating stall, and therefore mechanical failure during a stall event is not instantaneous [4]. Nonetheless, this study focuses on the effect of pressure pulses on a large tunnel and metro fan. Such fans are installed inside vertical airways that connect the main underground tunnels with the external environment, so they are not directly exposed to the passage of the trains in the main tunnel. They are typically subjected to a variation of the volume flow as an indirect effect of the passage of one or more trains, after a series of reflections and interactions of pressure waves inside the system of underground passages.

Literature reports on the effects of trains inside underground systems focusing mainly on the prediction of pressure waves inside the tunnels and on the variation of drag on the trains when entering, leaving or passing through a station. Little is reported on the direct effects of pressure waves on the ventilation system and in particular on the performance of fans. Vardy [5] experimentally investigated pressure waves in an underground station on London Transport's Victoria Line, giving an insight of how the velocity field is affected by the passage of a single train at different positions inside the main tunnel and in the secondary airways. The same author [6] derived an analytical model to predict the variation of drag and skin friction on the train as a function of the blockage ratio when it enters or leave a station. Bellenoue et al. [7] experimentally and numerically investigated the compression wave that originates when a high-speed train enters an underground station. William-Louis and Tournier[8] proposed and validated a method for predicting the evolution of pressure in underground tunnels with one or more trains. Recently, Huang et Gao[9] developed, tested and validated a dynamic layering CFD method for the prediction of unsteady flows inside subway tunnels, focusing on underground systems with natural and forced ventilation.

To cope with the effects of a transient change of volume flow rate and fluctuating pressure through fans, tunnel ventilation fan designers have classically utilised one of three approaches during the selection [4]. The first strategy, a fan with a non-stalling blade angle, is the most conservative selection strategy. The second strategy, a fan with a high enough pressure developing capability to operate with a pressure pulse without stalling, works well with smaller pressure pulses. The third strategy, a fan with a fitted stabilisation ring, works well with larger pressure pulses, allowing fan selection close to its peak aerodynamic efficiency and then effectively managing the mechanical consequences of driving into stall under the influence of pressure pulses.Nevertheless a proper understanding of the mechanisms generated on the fan by pressure fluctuations inside a tunnel or metro system is considered mandatory to address the selection of the main operating parameters of the current generation of axial flow fans and to obtain useful guidelines for the design of the next generation.

Here the effects of compression and expansion waves passing through a fan are computed by mean of a LES turbulence closure which is considered suitable of simulating (part of) the flow unsteadiness without fully accounting for the influence of turbulence spectrum. In view of the force unsteadiness on the fan blades, the simulation of the unsteady aerodynamics is the key ingredient to dissect the load evolution during the pressure pulse transient. Proper LES solutions are hardly available in the open literature due to the formidable computational effort required for the solution of the turbulent spectrum up to the inertial sub-range [10]. To this end a viable strategy for turbomachinery flow is the reduction of the level of discretization to a very large eddy simulation (VLES), pro-

viding in most of the computational domain resolution sufficient to solve the larger turbulent scales [11], coupled with an appropriate sub-grid scale model (e.g. dynamic model of Germano [12] or one-equation sub-grid scale model [13]). This way, though the hypothesis of stationary, isotropic vortex cascade does not hold due to the insufficient discretization, the sub-grid scale model is able to account for the backscattering effect. The numerical methodology was routed on the open source philosophy, which has provided a new impetus in CFD code development [14]. The simulations have been carried out using OpenFOAM LES, already validated in turbomachinery and industrial flow predictions [15-23].

In the following, first, the test case is described by providing the key information on the fan and on the nature of the pressure wavefront. Then a description of the computational approach is given as well as a description of the numerical model. Finally, results of the computations are discussed by illustrating the transient evolution of static pressure on the fan blade, the modification of the three-dimensional vortical field and the load on the blade.

TEST CASE DESCRIPTION

Ventilation fan

The fan under investigation was a uni-directional 2.24 m diameter fan driven by a 4-pole motor at 1500 rpm. Figure 1 shows the 2.24 m prototype fan, designed for one-time only emergency operation at 400°C. The fan rotor selected for the present investigation was labeled 224 JFM. Table 1 specifythe geometrical data of the blade of 224 JFM fan.

Figure 1 – 224 JFM Fan

Table 1 - 224JFM fan blade data

Blade section	ARA-D	
Diameter at the tip	2240 mm	
Blade count	16	
Hub-to-tip ratio	0.5	
	Hub	*Tip*
Chord (mm)	143	92.5
Solidity (-)	0.64	0.21
Pitch angle (deg)	48	24

Air pressure fluctuations in tunnels

The pressure pulses are modeled, following [5] and [6], under the assumption that trains entering or leaving an underground station generate a series of pressure waves. In view of the pressure pulse magnitude, O(10^2) Pa, and duration, O(10^{-3}) s, it is possible to investigate the wavefronts either as rapid changes in a continuous flow or as an instantaneous pressure discontinuity according to the purpose of the analysis.

The focus on fan aerodynamic response (effect) under pressure wavefronts (cause) allows to use the latter approach, which models a sudden increase or drop of pressure as a variation of the bulk velocity inside the duct:

$$\Delta p_{pulse} \propto \Delta U_{bulk} \qquad (1)$$

Table 2 gives the details of the modelled pressure wave-fronts. With this simplification the pulse is considered quasi-instantaneous, as the variation of pressure is simulated as occurring in a time interval Δt_{ramp} of order $O(10^{-5})$ s, while the duration of the transient simulation Δt_{pulse} is of $O(10^{-3})$ s.

Table 2 -Description of the pressure pulses

Δp	±1000 Pa
Δt_{ramp}	1.3×10^{-5} s
Δt_{pulse}	4 ms

COMPUTATIONAL METHODOLOGY

Numerical technique

The computational analysis was based on the use of the open source finite volume C++ CFD code OpenFOAM 1.7.x. Here, the LES prediction of the fluid motion was computed by solving the filtered unsteady Navier-Stokes incompressible set of equations. LES was performed using the closure SGS model of Davidson [13], that requires to solve an additional transport differential equation forthe sub-grid turbulent kinetic energy k_{SGS}. In this model the k_{SGS} equation is solved to compute the velocity-scale of the sub-grid turbulence model. The equation reads as:

$$\frac{\partial k_{SGS}}{\partial t} + \frac{\partial k_{SGS}}{\partial x_j} = \frac{\partial}{\partial x_j}\left[\left(\nu + \nu_{SGS}\right) \frac{\partial k}{\partial x_j} \right] + P_{k_{SGS}} - \varepsilon_{k_{SGS}} \qquad (2)$$

In Eq. (2) the sub-grid scale viscosity is computed as follows:

$$\nu_{SGS} = < c_{SGS} >_{xyz} \sqrt{k_{SGS}}\,\Delta \qquad (3)$$

The coefficient $<c_{SGS}>$ is obtained with the well-known procedure ofdynamic Smagorinsky model [12]. Such SGS-model in its original formulation allows backscatter, i.e. to account for flowing of energy from small- to large-scale structures. Such capability was neglected in the original implementation of OpenFOAM but it is considered beneficial to partially account for the low-density of the computational grid. For this reason backscattering was restored in the model, limiting the lower negative values of SGS-viscosity to:

$$\min[\nu_{SGS}] \geq -\nu \qquad (4)$$

Computations were carried out using a central difference scheme with a TVD scheme to prevent numerical instabilities and a second-order implicit approach for time marching solution. Moreover although some TVD schemes introduce dissipation of high frequencies, this problem was not found to be significant in the presented formulation. Incompressible Navier-Stokes equations were solved using a ILU preconditioned semi-iterative conjugate gradient (CG) linear solver, in combination with a PISO segregation scheme. The convergence threshold was set to 10^{-8} for the solution of the algebraic CG and to 10^{-5} for the PISO algorithm.The rotating flow field is solved in the relative frame of reference, taking into account the effects of Coriolis and centrifugal forces with an in-house version of the *pisoFoam* solver.

Numerical grid and boundary conditions

The computations here presented take into account the operation of the 224 JFMfan with a 24deg pitch angle. Reynolds number, based on the tip diameter and speed is 26.1×10^6. The computational domain extends half a chord upstream of the leading edge of the rotor and one chord downstream the trailing edge of the blade, as shown in Figure 2. The mesh is built with about 9 million hexahedral cells distributed with a block-structured topology. Concerning the distribution of the elements, in the axial direction it consists of 16%, 50% and 34% of nodes respectively upstream of the leading edge, in the blade passage and downstream from it. Moreover, 55 grid nodes are used to model the tip-clearance along the span. Additional details are given in Table 3. The mesh was clustered toward solid boundaries, with the ratio of minimum grid spacing on solid walls to mid-span blade chord set as 7×10^{-4} on the blade tip, casing wall and blade surfaces. The adopted grid refinement towards the solid surfaces controls the normalised wall distance y+ value about 1 on the first nodes row. The boundary conditions that were used are resumed in Table 4.

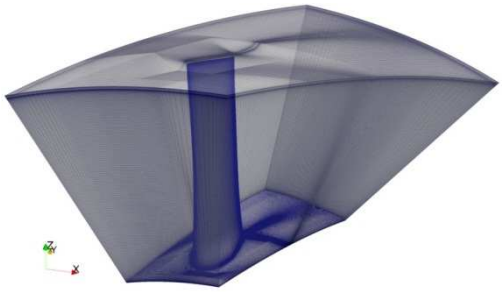

Figure 2 – computational domain.

Table 3 Fan mesh data

Nodes	9,021,968
Cells	8,862,550
Tip gap nodes	60,753
Tip gap cells	52,000
Blade surface cells	62,450
Average cell aspect ratio	1.34

Table 4 Boundary conditions

Inflow	Velocity profile with ±4.8% variation of U_{bulk} to simulate the effect of pressure pulse following eqn. (1)
Outflow	zeroGradient on all quantities
Rotor	Non-slip
Stator	$W=\omega R$
Periodic boundaries at mid-pitch	

RESULTS

Overall performance

In Figure 3 the effect of the two investigated pressure waves is shown with a plot of the evolution of the pressure-rise of the rotor stage over time. As the positive pressure wave-front hits the fan a sudden drop is recognizable due to choking. As the rotor adapts to the increase of volume flow, the pressure rise is recovered and the operating point moves to reach the equilibrium point on the characteristic curve. The effect of a negative wave-front is less drastic: a sudden pressure rise, that can be explained with the sudden increase of lift on the blade, is recognizable, after which the rotor adapts again to the new volume flow rate.

An insight of the rotor adapting to the change in volume flow rate is given in Figure 4, where the transient evolution of the operating points is shown against the experimental and numerical total pressure - volume characteristic curves. The points shown confirms the sudden pressure rise/drop due to the imposed quasi-instantaneous change in the mass flow rate. In the following analysis of the fan unsteady behaviours, the positive pressure pulse evolution will be discussed moving from A to C duty conditions, while the negative pressure pulse will take into consideration the points from A to E.

Remarks on blade loading

Figures 5 and 6 show the time evolution of the integral values of forces and moments on the blade during the increase or drop of flow rate. In the first case (Figure 5), as the blade stalls, the peripheral component of force is almost null, whereas the axial component shows a sudden change of sign. The second case, Figure 6, that corresponds to the drop of flow rate, leads to an overall overload of the blade, as the value of both axial and peripheral forces doubles.

Rotor flow under pressure pulses

The evolution of the rotor flow field under the effect of the two different wavefronts is shown in Figure 7 and 8. In Figure 7 the static pressure coefficient distribution over the suction surface of the blade is shown for the positive pressure wave case, together with plots at tip, midspan and hub to give an insight of the sudden increase of mass flow. Iso-contours of pressure coefficient show the sudden change of the pressure distribution during the pulse (label B) confirmed by pressure iso-lines over the suction side of the surface of the blade that show a clear 90 deg turning.

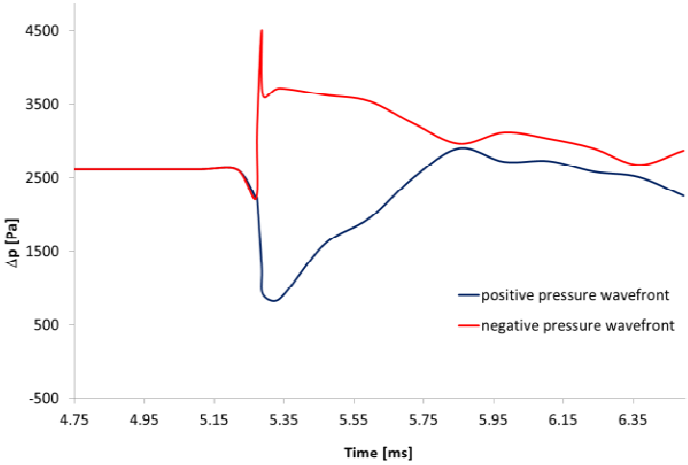

Figure 3 – Static pressure rise evolution after pressure pulses

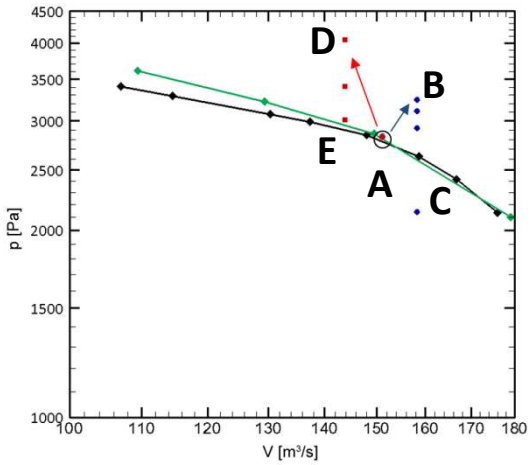

Figure 4 – Rotor's performance chart. Black line: exp characteristic curve, green line: CFD characteristics. Red and blue dots: operating points under negative and positive wavefronts.

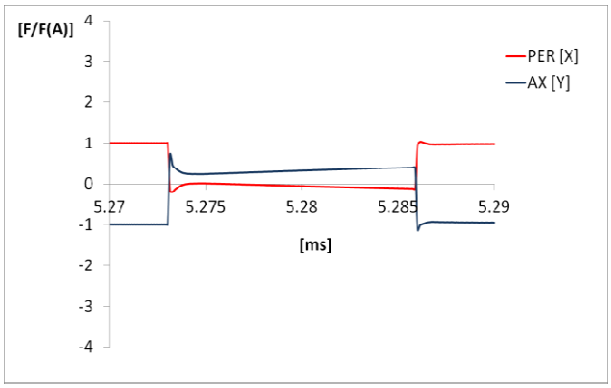

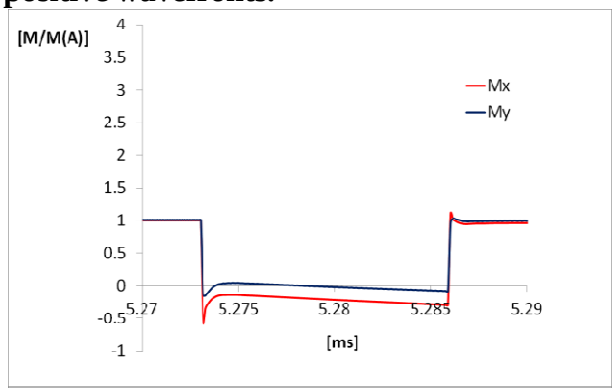

Figure 5 – Forces (left) and moments (right) on the blade vs time for positive pressure wave. Values are normalized w.r.t. the corresponding norm at instant "A".

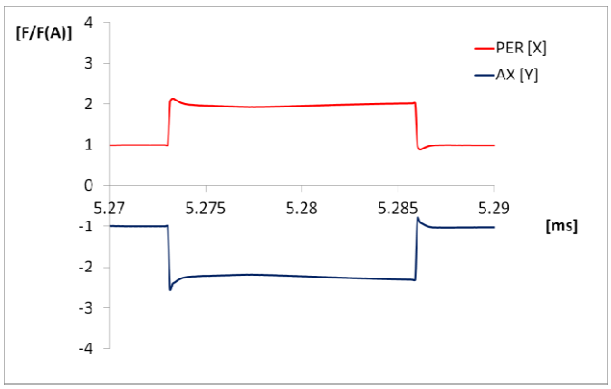

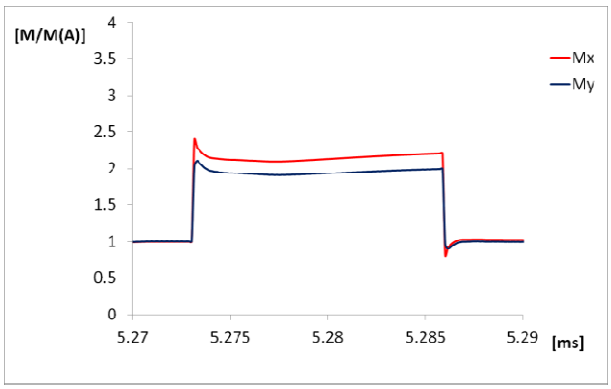

Figure 6 - Forces (left) and moments (right) on the blade vs time for negative pressure wave. Values are normalized w.r.t. the corresponding norm at instant "A".

Nevertheless the rotor adapts to the new volume flow rate (label C) quite quickly as shown from the evolution of C_p. As the rotor is working at operating point (A) or adjusting to the new volume flow rate (C) pressure-isolines are quasi-vertical and aligned with the blade span, whereas during pressure pulse (B) isolines are more radial and give evidence of a flow separation from the hub to 2/3 of the span, while the outer section, in proximity of the tip, is still capable of contributing to the rotor pressure developing capability. Distribution of the pressure coefficient show also that the blade is stalled during the pulse at midspan while is still able to provide lift at the tip and the hub.

Conspicuous data for the sudden drop of flow rate are shown in Figure 8 that reveals a different behaviour. As the pulse hits the blade the rotor adjust to the drop of mass flow increasing the work and so the lift over the blade. In this case the distribution of pressure isolines remains “vertical”, yet an increase of load at midspan is recognisable. Distributions of the pressure coefficient show that midspan and tip sections are over-loaded. At the hub the effect of the pressure wave is to recover the work capability of the blade, that in normal operations is compromised. In fact the design of the blade at the hub is constrained by mechanical requirements that do not allow an aerodynamic optimisation.

Examining the vortical structures that develop inside the vane, from the sequence of Q iso-surfaces analysed during the work (and not shown here due to lack of space) the large-scale structures are not clearly affected by the pulses. It is possible to speculate that this is due to the fact that the pressure wavefronts are associated with a timescale that is shorter than the one of large-scale structures and that the intrinsic coherence of such structures requires high energy change to be broken. Nevertheless the evolution of smaller scale structures at tip is partially unveiled in Figure 9. Here large-scale vortices such as the tip-separation vortex and the tip-leakage vortex maintain the aforementioned behaviour. On the contrary, smaller-scale structures such as the ones released from the trailing edge show recognizable differences from the two simulations, confirming that they are affected from the pulse with a comparable time-scale.

CONCLUSIONS

This paper presented results of LES computations that were carried out on a large tunnel ventilation fan subjected to a discontinuous pressure rise and drop reach the device. The effect of the incoming wave-fronts was simulated according to the assumption of a discontinuous change of the volume flow rate. The transient evolution of pressure rise was discussed, describing also the variation of the pressure field over the blade during the passage of the pressure wave-fronts. The evolution of small-scale vortical structures and the evolution of peripheral and axial forces over the blade were presented.

The transient evolution of pressure rise capability of the fan was discussed showing the change of the operating point and the adjustment to the change of volume flow rate. Results show that the device is able to quickly adjust to the new operating conditions and that the large-scale vortical structures released from the blade are not affected by the incoming wave-front.

On the contrary the sudden variation of volume flow rate affects the small-scale structures, that are characterised by a time-scale comparable with the one of the incoming pressure-wave.

Results show that the main effects of the wave-fronts are related with the variation of the static pressure field. In fact a sudden increase of the volume flow rate leads to a complete redistribution of the static pressure field over the blade span, leading to choking. On the contrary a sudden decrease of the flow rate results in an abrupt increase of the blade load, but in this case no span-wise redistribution of the static pressure over the blade is recognizable.

Finally at the investigated operating point the fan aerodynamics is not compromised by the incoming wave-fronts, but its mechanics is. In fact strong variations of the forces on the blade (and their moments) are observed: an increase of the flow rate results in a drop of the peripheral force and a change of sign of the axial force. Decrease of the volume flow rate on the contrary leads to a doubling of both components of the force acting on the fan blade.

ACKNOWLEDGEMENTS

The computing resources and the related technical support used for this work have been provided by CRESCO/ENEAGRID High Performance Computing infrastructure and its staff; see www.cresco.enea.it for information. CRESCO/ENEAGRID High Performance Computing infrastructure is funded by ENEA, the Italian National Agency for New Technologies, Energy and Sustainable Economic Development and by national and European research programs.

Part of the computations were carried out on PLX at CINECA, under *LESFAN* ISCRA project.

REFERENCES

[1] Sheard, A.G. & Jones, N.M., 2005, Emergency Ventilation for Vehicular, Rail and Metro Tunnels. Proc. Int. Congress: Safety Innovation Criteria Inside Tunnels, Dijon, Spain.
[2] Sheard, A. G., Corsini, A., Minotti, S., Sciulli, F., 2009, "The role of computational methods in the development of an aero-acoustic design methodology: application to a family of large industrial fans", CMFF'09, Sept 9-12, Budapest, Hungary, ISBN 978-963-420-984-3-0.
[3] Rippl, A. 1995, Experimentelle Untersuchungen zuminstationaren Betriebsverahhen an der Stabilitarsengenze eines mehrstudigen transsonischen Verdichters, PhD dissertation.

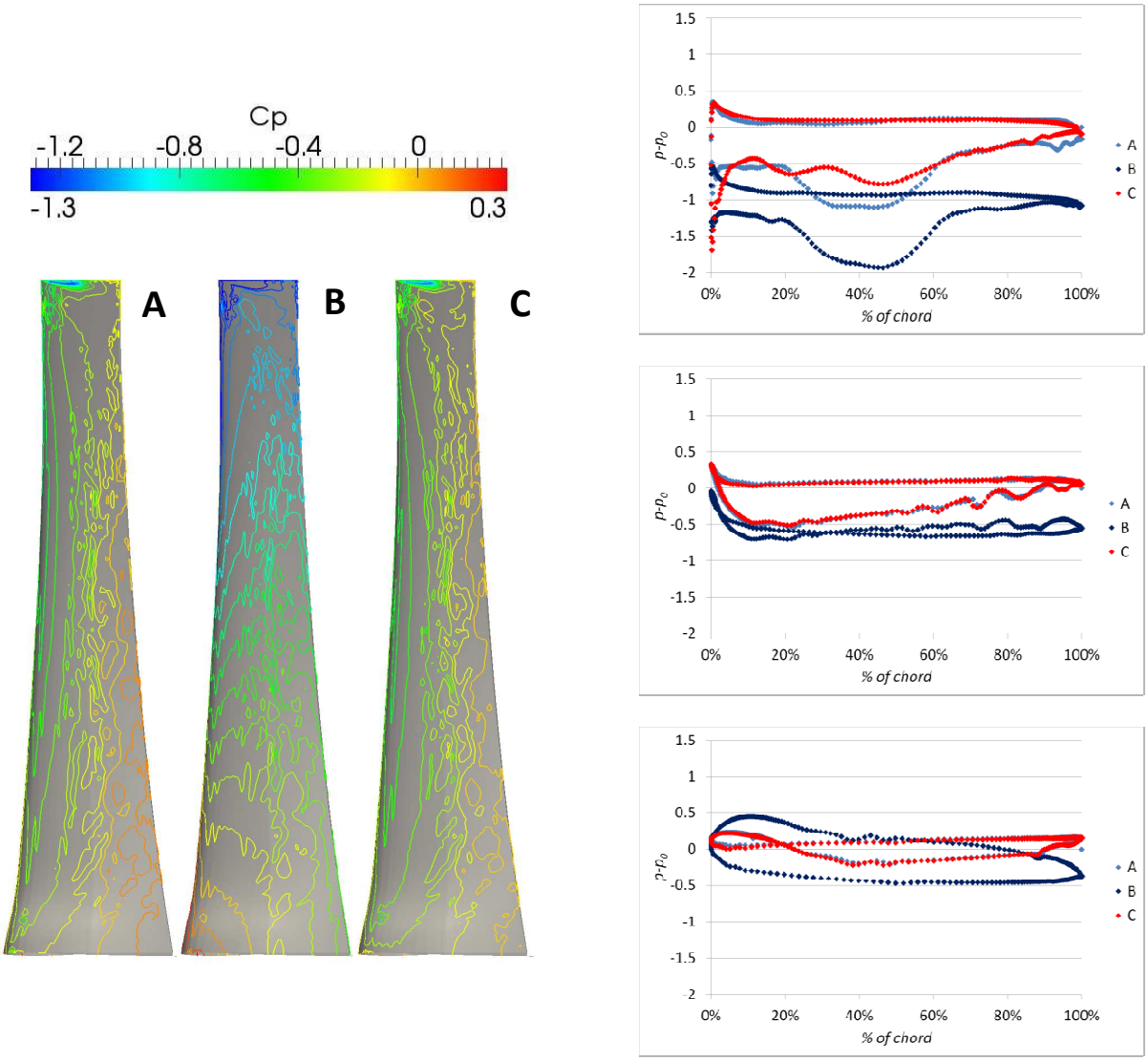

Figure 7 – Left: pressure coefficient on the suction surface of the rotor for instants A, B, C. Right: pressure coefficient along the blade at tip (top), midspan (middle) and hub (bottom).

[4] Sheard, A. G. and Corsini, A., 2012, The mechanical impact of aerodynamic stall on tunnel ventilation fans, Int. J. of Rotating Machinery, Vol. 2012.
[5] Vardy A. E., 1996, Aerodynamic drag on trains in tunnels Part 1: synthesis and definitions, Proceedings of the Institution of Mechanical Engineers, Vol 210, pp. 341-348.
[6] Vardy A. E., 1996, Aerodynamic drag on trains in tunnels Part 2: prediction and validation, Proceedings of the Institution of Mechanical Engineers, Vol 210, pp. 349-358.
[7] Bellenoue, M., Moriniere, V. and Kageyama, T., 2011, Experimental 3-d simulation of the Compression wave, due to train–tunnel entry, Journal of Fluids and Structures vol. 16(5), 581–595.
[8] William-Louis, M. and Tournier, C., 2005, A wave signature based method for the prediction of pressure transients in railway tunnels, Journal of Wind Engineering and Industrial Aerodynamics 93

(2005) 521–531.
[9] Huang, Y. and Gao, W., 2010, A numerical study of the train-induced unsteady airflow in a subway tunnel with natural ventilation ducts using the dynamic layering method, J. of Hydrodynamics, Vol. 22(2):164-172.
[10] Schneider , H., von Terzi, D., and Bauer H.-J., 2010, 'Large-Eddy Simulations of trailing-edge cutback film cooling at low blowing ratio', Int. J. Heat Fluid Flow, Vol. 31, pp. 767-77.
[11] Labois, M., and Lakehal, D., 2011, 'Very-Large Eddy Simulation (V-LES) of the flow across a tube bundle' Nuclear Engineering and Design, 241, pp. 2075–2085
[12] Germano, M., Piomelli, U., Moin, P. and Cabot, W. H., 1991, A Dynamic Subgrid-Scale Eddy Viscosity Model, Physics of Fluids A, Vol. 3, No. 7, pp. 1760-1765.

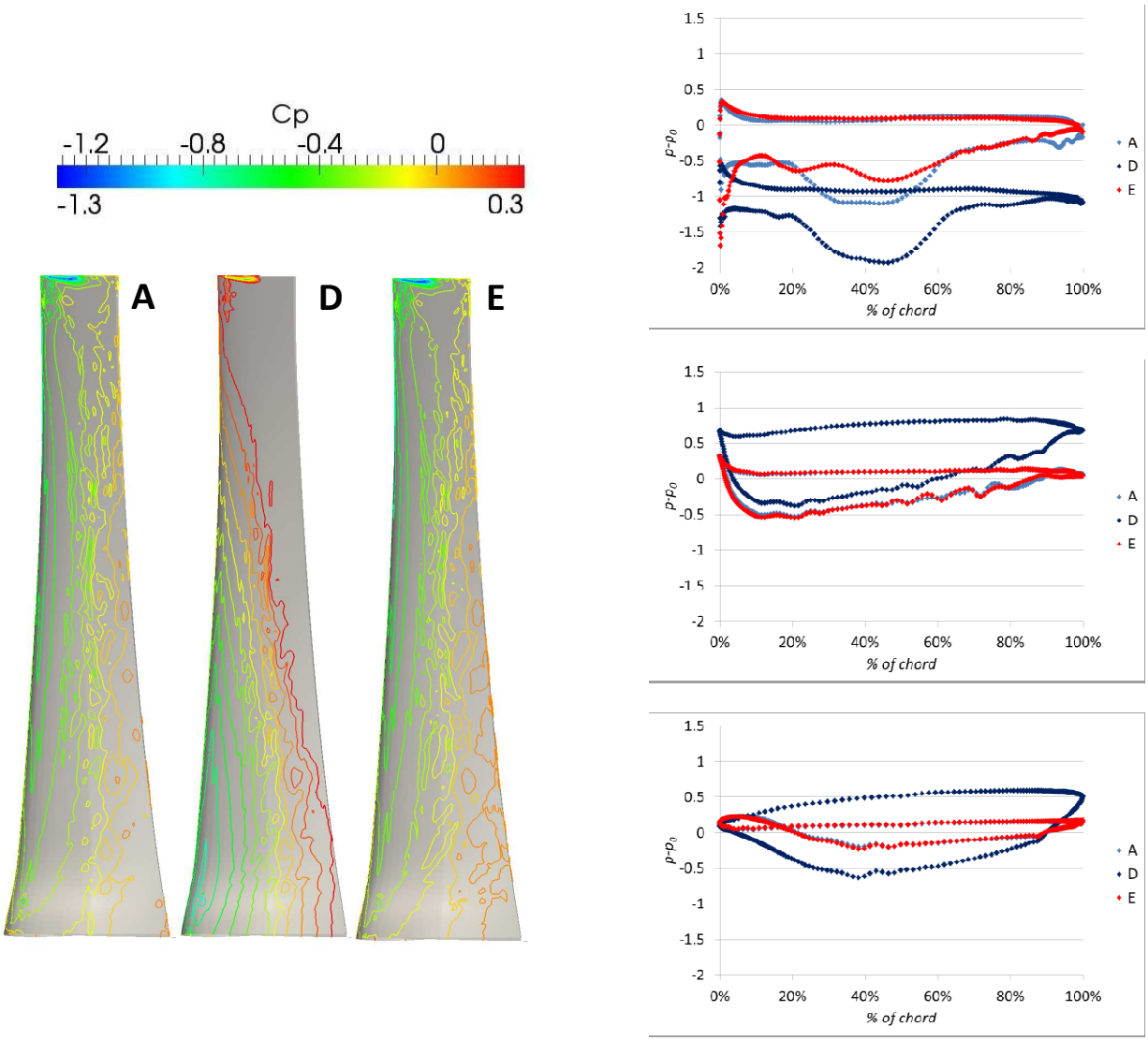

Figure 8 – Left: pressure coefficient on the suction surface of the rotor for instants A, D, E. Right: pressure coefficient along the blade at tip (top), midspan (middle) and hub (bottom).

[13] Davidson, L., 1997, Large eddy simulation: A dynamic one-equation subgrid model for three-dimensional recirculating_flows, 11th International Symposium on Turbulent Shear Flow, vol. 3, Grenoble, 1997; 26.1–26.6.
[14] Jasak, H., 2010, OpenFOAM: A year in review, 5th OpenFOAM Workshop, Gothenburg.
[15] Borello., D., Corsini, A., Rispoli, F., Sheard, A.G., 2011, "DES of a Large Industrial Fan at Design Operation", submitted to Journal of Power and Energy.
[16] Borello., D., Corsini, A., Rispoli, F., Sheard, A.G., 2012, "LES of the aerodynamics and aero-acoustic performance of an industrial fan designed for tunnel ventilation", draft submitted to Turbo

Expo 2012, ASME paper GT2012-69046.

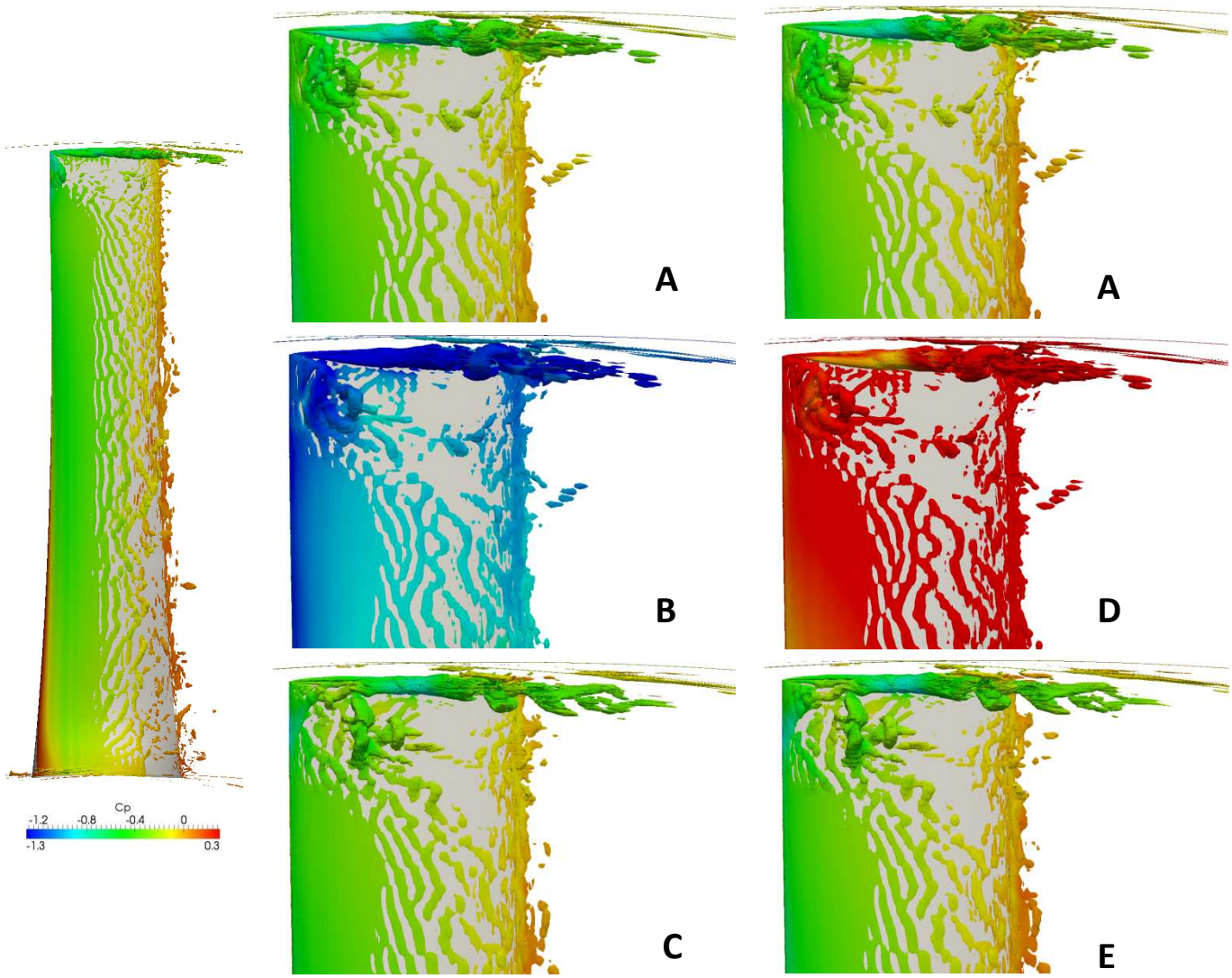

Figure 9 – Turbulent structures visualized with isosurfaces of Q=10,000 colored with pressure coefficient. An over-all visualization of the blade at instant A is given in (left). Tip region is shown at different instants (see labels) for positive (middle) and negative (right) wavefronts.

[17] Corsini A., Rispoli F., 2005, "Flow analyses in a high-pressure axial ventilation fan with a non-linear eddy viscosity closure", Int J Heat Fluid Fl, 17, pp. 108-155.
[18] Borello D., Hanjalic K. and Rispoli F., 2005, "Prediction of turbulence and transition in turbomachinery flows using an innovative second moment closure modelling", ASME Journal of Fluids Engineering, 127, pp.1059-1070.
[19] Borello D., Hanjalić K., Rispoli F., 2007, "Computation of tip-leakage flow in a linear compressor cascade with a second-moment turbulence closure", Int. J. Heat Fluid Flow, vol. 28.
[20] Borello, D., Delibra, G., Hanjalic, K. and Rispoli, F. 2009, "Large-eddy simulations of tip leakage and secondary flows in an axial compressor cascade using a near-wall turbulence model". Proc. IMechE Vol. 223 Part A: J. Power and Energy, pp. 645-655.
[21] Borello, D., Delibra, G., Hanjalić, K. and Rispoli, F., 2010, Hybrid LES/RANS study of turbulent flow in a low speed linear compressor cascade with moving casing. GT2010-23755.
[22] Delibra G., Borello D., Hanjalić K. and Rispoli F., 2009, "URANS of flow and endwall heat transfer in a pinned passage relevant to gas-turbine blade cooling", Int. J. Heat Fluid Flow, 30.
[23] Delibra G., Borello D., Hanjalić K. and Rispoli F., 2010, "A LES insight into convective mechanism of heat transfer in a wall-bounded pin matrix", 14th Intern. Heat Transfer Conference, 2010, Washington DC, USA.